Dynamic molecular ordering in multiphasic nanoconfined ionic liquids detected with time-resolved diffusion NMR

Marina Karagianni[1], Lydia Gkoura[2], Amit Srivastava[3], Aris Chatzichristos[3], Nikolaos Tsolakis[1], George Romanos[1], Savvas Orfanidis[1], Nikolaos Panopoulos[1], Saeed Alhassan[4], Dirar Homouz[3], Jamal Hassan[3*], Michael Fardis[1*], and Georgios Papavassiliou[1*]

Supplementary Information

Content:

Supplementary Methods

1. DSC and LN_2 porosimetry measurements

Differential Scanning Calorimetry (DSC) analysis (shown in the inset of Fig. 6a in the main article) was performed with a TA Instruments 2920 MDSC. The runs proceeded with a cooling down to −170 °C followed by heating up to 100 °C at a rate of 10 °C·min^{-1}.

Liquid Nitrogen (LN_2) porosimetry was performed with the Autosorb-1 MP (Quantachrome) Nitrogen Porosimeter. Before measurement, the pristine SBA-15 and MCM-41 samples were outgassed at 300^{o}C and high vacuum (10-5 mbar) for 24 hours, while for the IL-modified samples, the outgassing temperature was set to 90^{o}C. The DFT method (Calc. Model: N2 at 77 K on silica, cylindr. pore, NLDFT equilibrium model) was applied in the desorption branch of the isotherm to provide the pore size distributions of the pristine samples.

Nitrogen isotherms of the mesoporous silica materials MCM-41 and SBA-15 and of the corresponding $[BMIM]^+[TCM]^-$/MCM-41(SBA-15) ionogels are depicted in Supplementary Figure 1. The steep increase observed in MCM-41 and SBA-15 at low pressures indicates the formation of a nitrogen monolayer in the pore walls. The hysteresis loop observed in both samples is the result of N_2 evaporation from cylindrical pores open at both ends and of capillary condensation, which in SBA-15 occurs at higher relative pressure due to its larger pore size.

Regarding the $[BMIM]^+[TCM]^-$/SBA-15 ionogel no measurable amount of adsorbed nitrogen is detected, indicating complete filling of the pores with the IL. Notably, an appreciable amount of adsorption is observed in the $[BMIM]^+[TCM]^-$/MCM-41 ionogel. However, no reliable pore size distribution could be deduced from this measurement. At the same time, the relevant isotherms resemble those of nonporous silica[1], implying that the measured adsorbed volume might be related with nitrogen adsorption in the interparticle-space.

2. ^{1}H NMR spin-spin relaxation time T_2' measurements

2(i). The Hahn echo pulse sequence

The Hahn spin echo decay (SED) experiments were acquired with the typical ($\pi/2 - \tau - \pi - \tau -$ echo) pulse sequence, at various temperatures in constant magnetic field gradient G=34.7 Tm^{-1}. In the case of unrestricted diffusion such as the diffusion of [BMIM]$^+$ cations in the bulk RTIL, as illustrated in Supplementary Figure 3a, the SED is described by relation[2]

$$\frac{h(\tau,G)}{h(0)} = exp\left(-\frac{2\tau}{T_2}\right)\ exp\left(-\frac{2}{3}\gamma^2 G^2 D\tau^3\right) \qquad (1)$$

In the above expression $\frac{h(\tau,G)}{h(0)}$ is the normalized signal intensity, γ is the nuclear gyromagnetic ratio and D the self-diffusion coefficient.

2(ii). The CPMG pulse sequence

The typical CPMG pulse sequence consists of a $\pi/2$ pulse followed by a train of π-pulses ($\pi/2 - \tau - \pi - (2\tau - \pi)_n$), which generates an equal number of consecutive spin echoes at halfway between each π-pulse pair.

For unrestricted diffusion in a constant magnetic field gradient G the amplitude of the nth echo, formed at time $t = n \cdot (2\tau)$ is given as:

$$M(\tau,G) = M(0) \cdot exp\left[-\left(\frac{1}{T_2} + \frac{1}{3}\gamma^2 G^2 D\tau^2\right) \cdot t\right] = M(0) \cdot exp\left(-\frac{t}{T_2'}\right) \quad (2).$$

The spin echo decay (SED) decreases exponentially with the effective spin-spin relaxation rate $\frac{1}{T_2'} = \frac{1}{T_2} + \frac{1}{3}\gamma^2 G^2 D\tau^2$ (3)

The main panel in Supplementary Figure 2 shows the CPMG SED of bulk [BMIM]$^+$[TCM]$^-$ acquired at interpulse time spacing 2τ = 60μs and a number of 10000 pulses, at three representative temperatures: 297K, 353K, and 400K. The relevant $g(T_2')$ distributions shown in the inset of

Supplementary Figure 2 were acquired by inverting the CPMG spin echo envelope decay curves with a Tikhonov regularization algorithm[2,3], as described below.

Supplementary Figure 3b-3d illustrates the influence of the interpulse time spacing 2τ on the effective T_2' of the bulk IL $[BMIM]^+[TCM]^-$ at three representative temperatures 297K, 353K and 400K. This is in accordance with the second term of Supplementary Equation (3), which describes the dephasing of the transverse magnetization owing to diffusion in the presence of a constant magnetic field gradient. As the time spacing between consecutive π-pulses $2\tau \rightarrow 0$, the effect of diffusion becomes negligibly small. This effect is excellently demonstrated in the logarithmic plots of the SED envelopes in the insets of Supplementary Figures 3b – 3d. From these plots the self-diffusion coefficient *D* were evaluated accordingly by fitting the graph of $1/T_2'$ versus τ^2 to equation (2). The resulting *D* values at 297K, 353K and 400K are given in Supplementary Table 1. The corresponding intrinsic T_2 values were found to range between 200 and 500ms. To compensate the effect of diffusion in the SED during measurements of the T_2' in the main article, the interpulse time interval τ was set equal to 30 μs.

2(iii). Inversion of CPMG spin-echo amplitude envelope to acquire the T_2' distribution

The $g(T_2')$ distributions of the effective spin-spin relaxation times T_2' was derived by inverting the CPMG envelope decay with a 1-D Tikhonov regularization algorithm.

Specifically, the experimental CPMG echo amplitude envelope was modeled with a Fredholm integral equation of the first kind[3,4],

$$\frac{M(t)}{M(0)} = \int_0^{+\infty} k_0(T_2', t) g(T_2') d(log_{10} T_2') \qquad (4).$$

In the above relation $\frac{M(t)}{M(0)}$ is the normalized signal intensity and the Kernel function $k_0(T_2', t)$ is equal to $k_0(T_2', t) = exp\left(-\frac{t}{T_2'}\right)$. This equation is transformed into a discrete vector-matrix formulation $\mathrm{M} = \mathrm{K_0 g}$, which subsequently can be inverted by implementing a non-negative

Tikhonov regularization algorithm[3,4] to acquire $g(T_2')$, as nicely illustrated in the inset of Supplementary Figure 2.

3. ^{1}H NMR T_2' -resolved diffusion measurements

In order to record the diffusion at different T_2' relaxation windows, the pulse sequence shown in Supplementary Figure 4 was implemented. This comprises of a "Hahn echo"-part, encoding the effect of diffusion, followed by a CPMG pulse train with the protocol, $\pi/2 - \tau - \pi - \tau - (t_E - \pi - t_E)_n$.

The CPMG SED curves were recorded by varying τ (at constant t_E), and subsequently inverted to acquire the relevant $g(T_2')$ curves. The contour plots in Figures 2 and 3 in the main article are constructed by consecutive $g(T_2')$ curves, at progressively increasing delay time τ.

By recording the integral of each T_2' component vs. τ, the Hahn SED curves of each individual T_2' component is acquired, as illustrated in Figures 2b, 2d, 3b, and 3d of the main article. Since the various types of ILs cations (adsorbed, mobile confined, bulk) are characterized by distinctly different T_2', the diffusion dynamics of each component is imprinted in the time dependence of the relevant Hahn SED curves.

4. 2D ^{1}H NMR D-T_2' measurements

2D D-T_2' experiments were performed to unveil the presence of distinct diffusion processes in the RTIL confined in MCM-41 at elevated temperatures. The D-T_2' data were acquired with the same pulse sequence described in the preceding section and in Supplementary Fig. 4. In particular, the T_2' -encoding CPMG part of the pulse sequence generates data in the "direct" dimension, comprising the intensity of all CPMG echoes recorded simultaneously in a single shot. Data in the "indirect" dimension encoding the effect of diffusion are accumulated in successive experiments by incrementing the delay time τ in the value range from 30μs to 2000μs.

In the presence of a distribution of diffusion processes and relaxation times, the decay of the recorded D-T_2' signal intensity is described by equation[5-7]:

$$\frac{M(\tau,t)}{M(0,0)} = \iint_0^{+\infty} \left\{ \mathrm{e}^{-\frac{Dg^2\gamma^2\tau^3}{12}} e^{-\frac{\tau}{T_2}} \right\} \mathrm{e}^{-\frac{t}{T_2'}} f(D,T_2) dD dT_2 \quad (5)$$

In the case of very long T_2 values, as in our case, $\frac{\tau}{T_2} \ll 1$, and equation (5) transforms to the following simple form with separated variables:

$$\frac{M(\tau,t)}{M(0,0)} = \iint_0^{+\infty} \mathrm{e}^{-\frac{Dg^2\gamma^2\tau^3}{12}} \mathrm{e}^{-\frac{t}{T_2'}} f(D,T_2) dD dT_2 \quad (6)$$

Equation (6) was subsequently inverted by means of a non-negative 2D Tikhonov regularization algorithm to acquire the distribution function $f(D,T_2)$[5,8,9].

5. Computational methods

DFT calculations

Geometry optimizations and frequency analysis were performed using the ORCA suite of programs[10,11]. Three minimum energy configurations were found; 1) $[TCM]^-$ forming hydrogen bonds between one of its nitrogen atoms with the silanol groups of the surface, 2) $[TCM]^-$ forming hydrogen bonds between two of its nitrogen atoms with the surface, and 3) $[TCM]^-$ forming hydrogen bonds between three of its nitrogen atoms with the surface (Supplementary Table 2, Supplementary Figure 5). According to the energy calculations, the most stable configuration is the one where $[TCM]^-$ forms hydrogen bonds between two of its nitrogen atoms (Supplementary Figure 5b) with the surface. In this case, the Butyl- "tail" of the $[BMIM]^+$ is pointing away from the surface of the silica, thus filling the pore space, in good agreement with experimental results[1]. Using the optimized geometry, desorption and dissociation energies of the adsorbed IL were calculated (Supplementary Table 3). Considering the energy and enthalpy values, the desorption of the $[BMIM]^+[TCM]^-$ ion pair as whole is more favorable than the dissociation of the $[BMIM]^+$ cation alone.

To examine desorption of the IL from the silica surface, *Ab Initio* Molecular Dynamics (AIMD) simulations were conducted using the ORCA suite of programs[10,11]. The Silica-RTIL system was left to equilibrate for 1500 iterations at 300K and 400K. Time-averaged values of selected representative atomic distances (Supplementary Figure 6) are recorded in Supplementary Table 4.

MD calculation of the Self-Diffusion coefficient

Due to the confinement geometry, the diffusion is minimal in the radial direction. Therefore, here, we consider only the axial self-diffusion coefficient. The mean squared displacement (MSD) of cations was calculated using

$$\langle \Delta z^2(\tau) \rangle = \frac{1}{N} \sum_{i=1}^{N} \langle [z_i(\tau + \tau') - z_i(\tau')]^2 \rangle_{\tau'} \quad (7)$$

where τ is the time difference, τ' is the time at the origin, and N is the number of cations. MSD was calculated over a time interval of 1.0 ns at a sampling rate of 1.0 ps. MSD was then averaged over 100 such time intervals. To estimate the self-diffusion coefficient, we fitted the MSD function with different regimes corresponding to different time scales. The algorithm fits the MSD to a continuous piece-wise function and finds the breakpoints which separate different modes of motions. The function we used for fitting is given by,

$$f(\tau) = \begin{cases} A_0 + B_0\tau^2 & ; \quad \tau < \tau_0 \\ A_1 + B_1\tau^{\kappa} & ; \tau_0 < \tau < \tau_1 \\ A_2 + B_2\tau & ; \quad \tau > \tau_1 \end{cases} \quad (8)$$

where $\tau < \tau_0$ corresponds to ballistic diffusion, $\tau_0 < \tau < \tau_1$ corresponds to crossover regime, and $\tau > \tau_1$ corresponds to Fickian diffusion.

Bulk MD Simulation

To calculate the diffusion coefficient of $[BMIM]^+$ cations in bulk, we run the MD simulation for Bulk system. The MD protocols and force-field parameters of IL, used for simulation is already presented in the main text. The MD simulation performed at room temperature at atmospheric

pressure. The density of our simulated system is 1.069 (±0.0005) gr cm^{-3}. The calculated density agrees with the experimental data. Since the system is bulk, here we have calculated the radial diffusion coefficient of cations using the Einstein relationship:

$$D = \frac{1}{6} \lim_{t\to\infty} \frac{d}{dt} \langle |r_i(t) - r_i(0)|^2 \rangle \qquad (9)$$

The snapshot of our simulated bulk system is shown in Figure S7. The calculated self-diffusion coefficients value is listed in Table S5.

Supplementary Figures (Fig. 1-7)

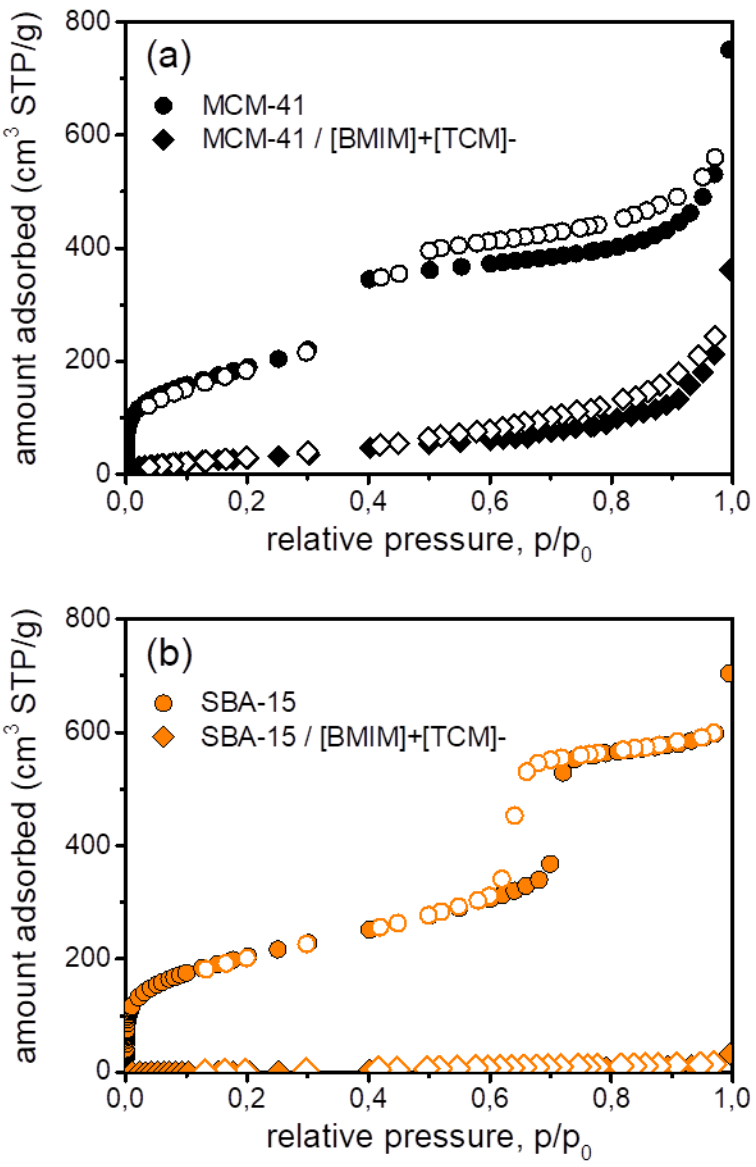

Supplementary Figure 1 | Porosimetry measurements at 77 K in MCM-41 and SBA-15 mesoporous silica materials before and after IL impregnation. (**a**) Nitrogen adsorption - desorption isotherms in MCM-41 and $[BMIM]^+[TCM]^-$/MCM-41. (**b**) Nitrogen adsorption - desorption isotherms in SBA-15 and $[BMIM]^+[TCM]^-$/SBA-15 samples.

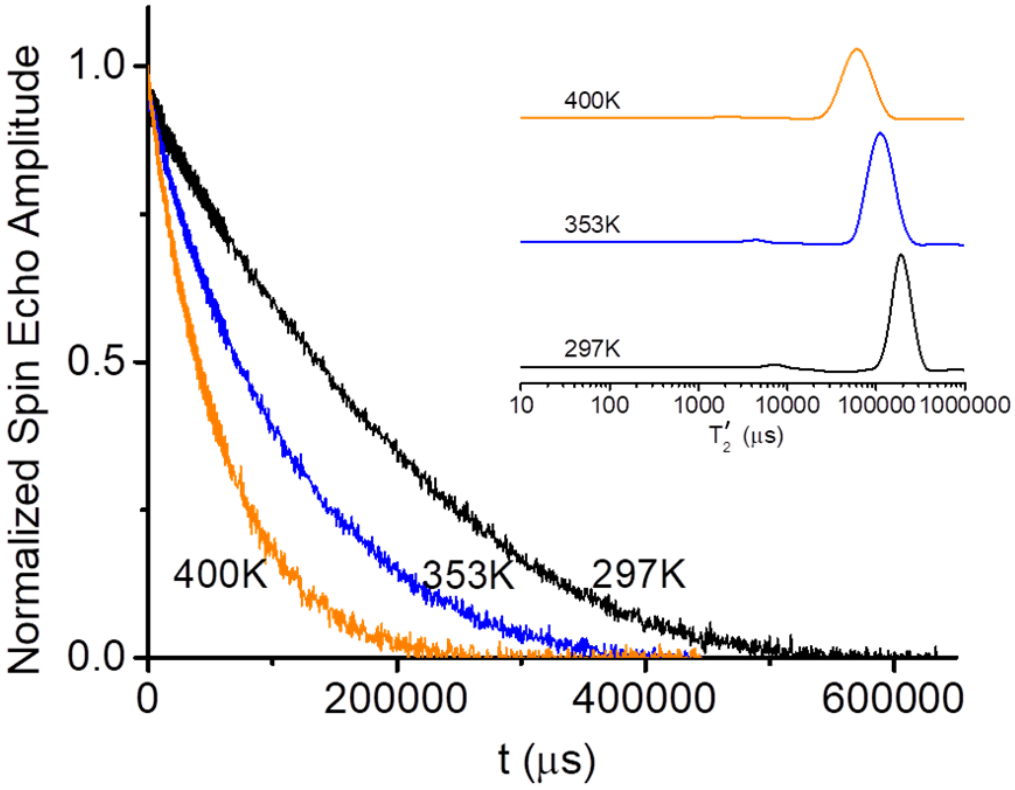

Supplementary Figure 2 | ^{1}H NMR CPMG spin-echo decay envelopes and the corresponding T_2' distributions. Representative CPMG spin-echo decay envelopes of bulk IL $[BMIM]^+[TCM]^-$ at 297 K (black line), 353K (blue line) and 400K (orange line). The experimental pulse sequence comprises of 10000 echoes with an interpulse separation of $2\tau = 60$ μs. The corresponding T_2' distributions are shown in the inset with the same colour mapping and were obtained by inverting the SED curves implementing a non-negative Tikhonov regularization algorithm.

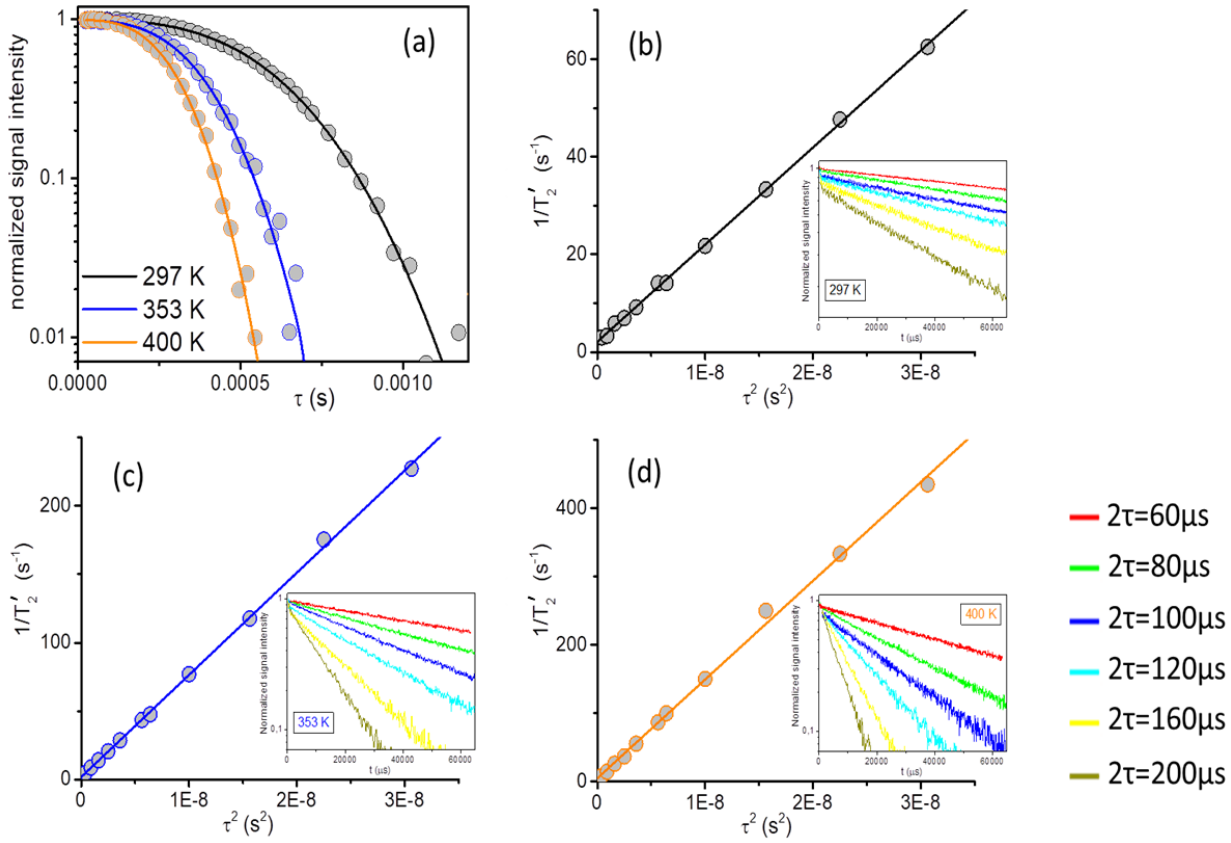

Supplementary Figure 3 | Calculating the ^{1}H NMR effective spin-spin relaxation time T_2' and self-diffusion coefficient D from the relevant CPMG and Hahn SEDsexperiments. **(a)** SED curves of bulk $[BMIM]^+[TCM]^-$ acquired with the Hahn pulse sequence at three different temperatures. The non-exponential decays follow the τ^3 law characteristic of unrestricted 3D diffusion. **(b)–(d)** Graphs of the effective dephasing rate $1/T_2'$ versus τ^2 for bulk $[BMIM]^+[TCM]^-$ measured with the CPMG pulse sequence for different interpulse spacing 2τ. Experimental results are shown for three different temperatures: 297K (**b**), 353K (**c**) and 400K (**d**). Semi logarithmic plots of the CPMG SED curves acquired at different interpulse intervals 2τ are shown in the insets with the corresponding color mapping indicated on the right.

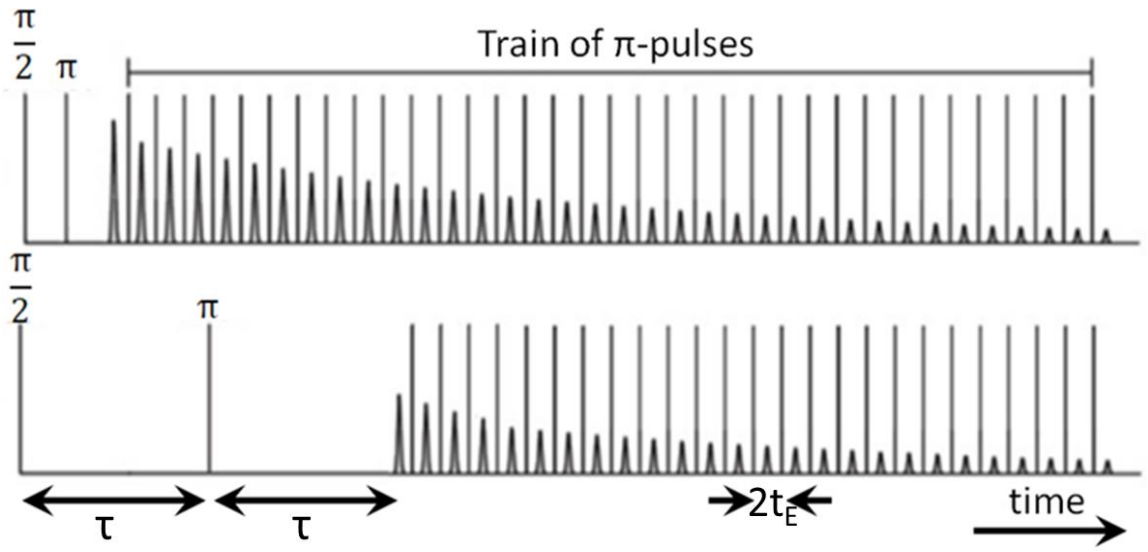

Supplementary Figure 4 | The NMR pulse sequence for recording diffusion effects at different relaxation windows. CPMG experiments were conducted by varying τ at constant t_E. (To minimize diffusion effects during the CPMG part of the experiment t_E was set equal to 30μs). The CPMG SED signal intensity was recorded at each experiment and subsequently inverted with a Tikhonov regularization algorithm. The signal intensity (integral area) of each T_2' component was then recorded vs. τ (T_2' resolved Hahn SED).

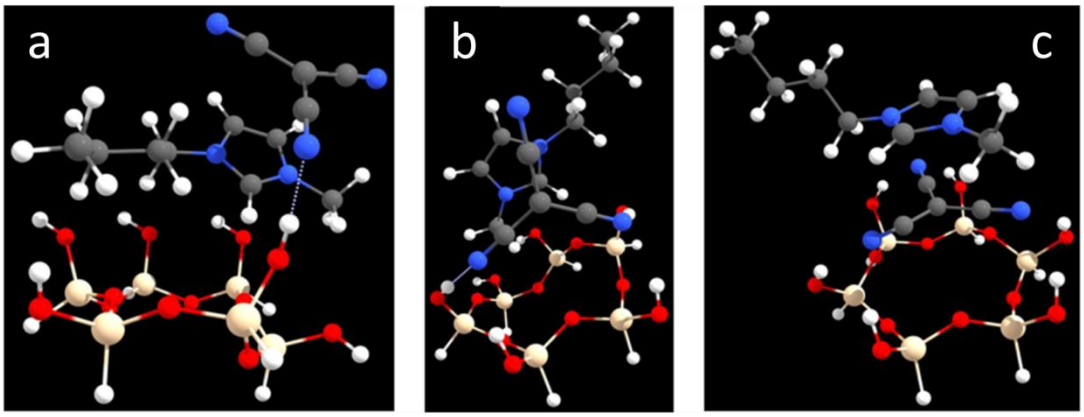

Supplementary Figure 5 | Geometries of energy minima of the [BMIM]$^+$[TCM]$^-$ - protonated [Si_6O_{12}] cluster system. Blue: nitrogen, grey: carbon, white: hydrogen, yellow: silicon, red: oxygen. Three configurations were found, with hydrogen bonds being formed between one (**a**), two (**b**) and three (**c**) nitrogen atoms of the [TCM]$^-$ and the silanols of the silica surface. The most stable, according to Supplementary Table 2, is the one presented in Supplementary Figure 5b (two nitrogen-bonding).

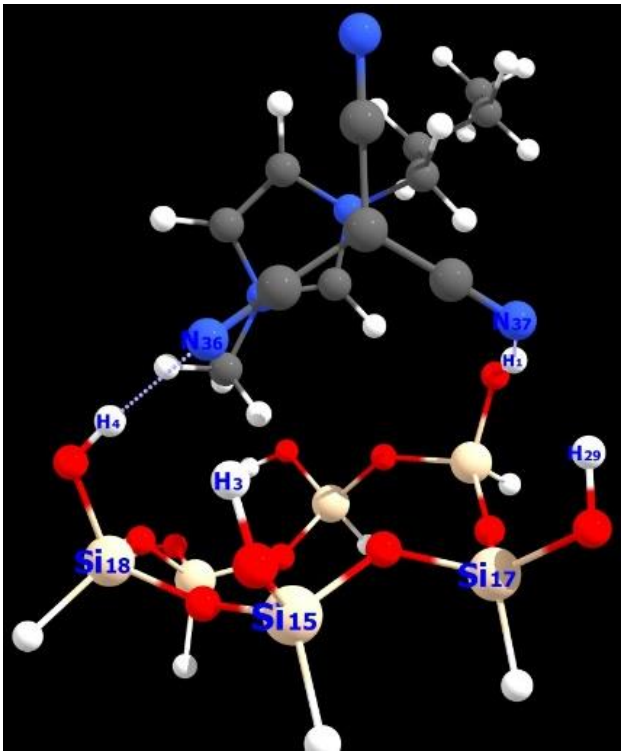

Supplementary Figure 6 | Atom labeling for measuring atomic distances representative of the desorption dynamics of the $[BMIM]^+[TCM]^-$ - protonated $[Si_6O_{12}]$ cluster system. Distances are presented in Supplementary Table 4. Blue: nitrogen, grey: carbon, white: hydrogen, yellow: silicon, red: oxygen.

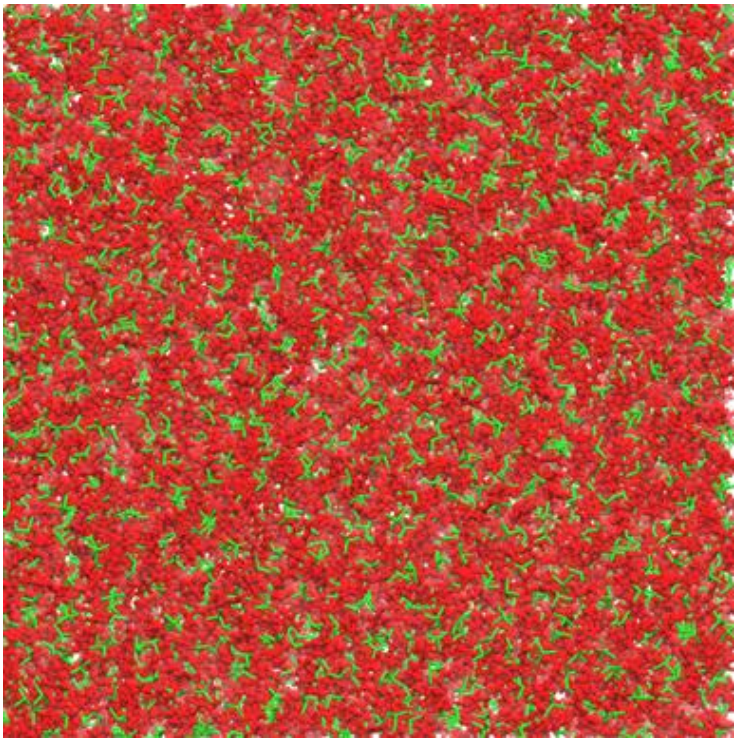

Supplementary Figure 7 | Snapshot of MD simulation of bulk [BMIM]$^+$[TCM]$^-$ at 300 K. In red color [BMIM]$^+$ are shown and in green color [TCM]$^-$.

Supplementary Tables (Table 1-5)

***T* (K)**	***D* (10^{-11} $m^2 \cdot s^{-1}$)**
297K	6
353K	26
400K	50

Supplementary Table 1 | Self-Diffusion coefficient *D* of bulk $[BMIM]^+[TCM]^-$ at 297K, 353K and 400K acquired from plots in Supplementary Fig. 3. The *D* values were acquired by Supplementary equation (2), from the slope $\frac{1}{3}\gamma^2 G^2 D$ of the straight lines.

Optimized geometries	**Energy (E_h)**
a) 1 Nitrogen-Bonding	-3382,16116990975
b) 2 Nitrogens-Bonding	-3382,17710736146
c) 3 Nitrogens-Bonding	-3382,15943908860

Supplementary Table 2 | Energies of the three optimized $[BMIM]^+[TCM]^-$ - protonated $[Si_6O_{12}]$ cluster conformations presented in Supplementary Figure 5. These are characterized by one, two, and three $[TCM]^-$ nitrogen atoms bonding with the $[Si_6O_{12}]$ surface. The conformation with 2 nitrogens-bonding corresponds to the one with minimum energy. Energy values are given in Hartrees.

Optimized geometry with two TCM^- nitrogen-atoms, forming hydrogen bonds with silanol groups	
$\Delta E_{desorption}$	24.81 Kcal/mol
$\Delta E_{dissociation}$	71.55 Kcal/mol
$\Delta H_{desorption}$	23.40 Kcal/mol
$\Delta H_{dissociation}$	70.27 Kcal/mol

Supplementary Table 3 | Desorption and Dissociation energies of the $[BMIM]^+[TCM]^-$ - protonated $[Si_6O_{12}]$ cluster system with optimized geometry.

	300K	**400K**
N37 - H1	1,9Å	2,0 Å
N37 - H29	3,4 Å	4,4 Å
N36 - H3	2,2 Å	2,4 Å
N36 - H4	2,4 Å	3,0 Å
N37 - Si17	4,5 Å	5,2 Å
N36 - Si15	3,8 Å	4,0 Å
N36 - Si18	4,2 Å	4,6 Å

Supplementary Table 4 | Time-averaged values of selected atomic distances at temperatures of 300K and 400K. Distances are illustrated in Supplementary Figure 6**.**

Conc.	Temp.(K)	Shell (nm)	D (10^{-11} m^2/s)	κ	A_1	A_2	B_1	B_2	τ_1 (ps)
MCM-41 Low	300	0 - 2.0	0.55	0.4101	0.289	0.615	0.061	0.0011	198
	400	0-2.0	1.75	0.4283	0.505	1.571	0.181	0.0035	200
MCM-41 High	300	0-0.49	0.65	0.4411	0.209	0.541	0.053	0.0013	150
	300	1.3-2.0	0.25	0.3719	0.142	0.297	0.034	0.0005	80
	400	0-0.49	5.6	0.6166	0.976	1.563	0.053	0.0112	192
	400	1.3-2.0	4.4	0.6766	0.655	1.397	0.068	0.009	164
Bulk	300		2.5	0.4872	0.5685	0.9300	0.0495	0.0015	211

Supplementary Table 5 | The fitting parameters for MSD based on MD simulations at different temperatures and concentrations. The fitting model function is described in Section 5.

Supplementary References

1. Stefanopoulos, K. L. *et al.* Investigation of Confined Ionic Liquid in Nanostructured Materials by a Combination of SANS, Contrast-Matching SANS, and Nitrogen Adsorption. *Langmuir* **27**, 7980–7985 (2011).
2. Kimmich, R., Unrath, W., Schnur, G. & Rommel, E. NMR measurement of small self-diffusion coefficients in the fringe field of superconducting magnets. *Journal of Magnetic Resonance (1969)* **91**, 136–140 (1991).

3. Mitchell, J., Chandrasekera, T. C. & Gladden, L. F. Numerical estimation of relaxation and diffusion distributions in two dimensions. *Progress in Nuclear Magnetic Resonance Spectroscopy* **62**, 34–50 (2012).
4. Day, I. J. On the inversion of diffusion NMR data: Tikhonov regularization and optimal choice of the regularization parameter. *Journal of Magnetic Resonance* **211**, 178–185 (2011).
5. Gkoura, L. *et al.* The peculiar size and temperature dependence of water diffusion in carbon nanotubes studied with 2D NMR diffusion–relaxation D–T_{2eff} spectroscopy. *Biomicrofluidics* **14**, 034114 (2020).
6. Hassan, J. *et al.* Ultrafast Stratified Diffusion of Water Inside Carbon Nanotubes; Direct Experimental Evidence with 2D D–T_2 NMR Spectroscopy. *J. Phys. Chem. C* **122**, 10600–10606 (2018).
7. Hurlimann, M. D. & Venkataramanan, L. The diffusion-spin relaxation time distribution function as an experimental probe to characterize fluid mixtures in porous media. *J. Chem. Phys.* **117**, 10223–10232 (2002).
8. d'Eurydice, M. N. & Galvosas, P. D–T_2 correlation using the inhomogeneity of single sided NMR devices. *Microporous and Mesoporous Materials* **205**, 40–43 (2015).
9. Nogueira d'Eurydice, M. & Galvosas, P. Measuring diffusion–relaxation correlation maps using non-uniform field gradients of single-sided NMR devices. *Journal of Magnetic Resonance* **248**, 137–145 (2014).
10. Neese, F. The ORCA program system. *WIREs Comput Mol Sci* **2**, 73–78 (2012).
11. Neese, F. Software update: the ORCA program system, version 4.0. *WIREs Comput Mol Sci* **8**, (2018).